Transforming an Insulating Metal–Organic Framework (MOF) into Semiconducting MOF/Gold-Nanoparticle and MOF/Polymer/Gold-Nanoparticle Composites to Gain Electrical Conductivity

Monica A. Gordillo,[†] Paola A. Benavides,[†] Kaikai Ma,[‡] and Sourav Saha[†,*]

[†]Department of Chemistry, Clemson University, 211 S. Palmetto Blvd., Clemson, SC 29634, USA
[‡]Department of Chemistry, Northwestern University, 2145 Sheridan Road, Evanston, IL 60208, USA
*Email: souravs@clemson.edu

ABSTRACT

Transforming permanently porous but electrically insulating metal–organic frameworks (MOFs) into electrically conducting materials is key to expanding their utility beyond traditional guest storage, separation, and delivery applications into the realms of modern electronics and energy technologies. To this end, herein, we have converted a highly porous but intrinsically insulating NU-1000 MOF into semiconducting NU-1000/gold-nanoparticle (AuNP) and NU-1000/polydopamine/AuNP composites via MOF- and polymer-induced reduction of infiltrated Au^{3+} ions into metallic AuNPs. The NU-1000/AuNP and NU-1000/PDA/AuNP composites not only gained significant room temperature electrical conductivity (~10^{-7} S/cm), which was ca. 10^4 times greater than any MOF/metal-nanoparticle (MNP) composites exhibited thus far under the same conditions, i.e., without photo- and thermal induction, but also retained sizable porosity and surface areas (1527 and 715 m^2/g, respectively), which were also larger than most intrinsically conducting 3D MOFs developed to date. The markedly higher conductivities of NU-1000/AuNP and NU-1000/PDA/AuNP composites can be attributed to more efficient charge hopping or tunneling through well-dispersed AuNPs embedded inside the crystalline MOF matrix, which pristine NU-1000 lacked. Thus, this work presented an effective new strategy to transform porous but non-conducting MOFs into electrically conducting MOF/MNP composites with considerable porosity, which could be useful in future electronics, electrocatalysis, and energy storage devices.

Keywords: metal–organic frameworks, gold nanoparticle, polydopamine, electrical conductivity, charge hopping

INTRODUCTION

Owing to their highly ordered porous structures that can be tailored for various guest entities ranging from small molecules to large polymers and nanoparticles, metal–organic frameworks (MOFs) have emerged as one of the most attractive and versatile functional materials of the 21st century.[1–2] Recently, electrically conducting MOFs[3–10] have attracted significant attention because of their diverse potential applications in modern electronics and energy technologies,[11–35] including batteries,[18–20] supercapacitors,[21–25] transistors,[26,27] chemiresistive sensors,[28–34] and electrocatalysis.[35–41] Although the porosity of MOFs is a key to their well-documented guest separation, storage, delivery, and sensing applications,[42–61] it also hinders long-range charge conduction through spatially separated redox-active components and thus causes poor intrinsic electrical conductivity of most porous MOFs. However, the porosity of MOFs could be exploited to create guest-induced electrical conductivity by introducing appropriate guest entities that can supply charge carriers and facilitate charge movement.[62–71] Nevertheless, since most small molecular guests are also intrinsically insulating, in order to create adequate guest-induced electrical conductivity, oftentimes

the host MOFs must be saturated with guests, which quash the porosity, i.e., the guest-induced conductivity of MOFs is often achieved at the expense of their porosity. In contrast, recent studies have revealed that polymeric guests formed inside porous MOF via *in situ* polymerization of pre-loaded monomers can not only improve the structural stability and porosity of certain collapse-prone frameworks,[72–74] but also introduce large number of functional groups that can create new properties and functions in the resulting MOF/polymer composites. For example, *in situ* generated conducting polymers (CPs) have transformed insulating MOFs into semiconducting MOF/CP composites,[75–80] MOF/polymer composites have been used to extract heavy metal ions, such as Hg, Au, Pb, and Pd ions, from aqueous solutions,[81,82] and a MOF/polydopamine/Pd-nanoparticle composite was able to catalyzed Suzuki coupling reaction.[73] However, the electrical conductivity of MOF/polymer/metal-nanoparticle (MNP) composites has been largely unexplored. Although an intrinsically insulating Rb-cyclodextrin (Rb-CD) MOF reduced infiltrated Ag^{+} ions to yield a Rb-CD/AgNP composite, it displayed negligible room temperature electrical conductivity (~10^{-11} S/cm) in the absence of light, but modest photo- and thermal conductivity (~10^{-7} S/cm) only after light and/or heat activation.[83] Therefore, we envisioned that porous but intrinsically insulating MOFs could be converted into electrically conducting MOF/MNP and MOF/Polymer/MNP composites by introducing relatively small amounts of guest polymers and MNPs that can facilitate long-range charge hopping and tunneling while also preserving significant porosity and surface area of the host framework.

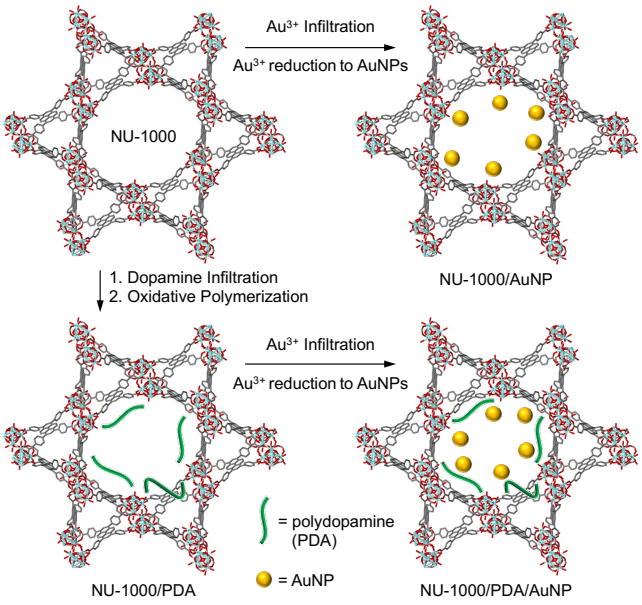

Figure 1. Transformation of NU-1000 to NU-1000/AuNP, NU-1000/PDA, and NU-1000/PDA/AuNP composites.

Herein, we demonstrate for the first time that a permanently porous but electrically insulating Zr-pyrene-tetrabenzoate (TBPy) MOF, called NU-1000,[84] can be converted into semiconducting MOF/AuNP and MOF/polydopamine/AuNP composites having significant electrical conductivity (Figure 1) via MOF and polydopamine (PDA) induced reduction of infiltrated Au^{3+} ions into metallic AuNPs. PDA was chosen for this purpose because (i) it can be synthesized easily inside MOFs via aerobic oxidative polymerization of infiltrated dopamine monomers[72,73] and (ii) it bears a large number of strong reducing groups, such as catechol and amines that are known to reduce Ag^{+}, Hg^{2+} and Pd^{+2} metal ions to corresponding metal

nanoparticles,[73,81,82] prompting us to envision that it should also be able to reduce infiltrated Au^{3+} ions into metallic AuNPs. Powder X-ray diffraction (PXRD) analysis revealed the crystallinity, structural stability, and the presence of crystalline AuNPs in NU-1000/AuNP and NU-1000/PDA/AuNP composites, which was further confirmed by scanning-electron microscopy (SEM) and scanning transmission electron microscopy coupled with energy dispersive X-ray (STEM-EDX) analyses revealing the coexistence of signature elements (Zr, N, and Au) of each component of the composites. Thermogravimetric analysis (TGA) revealed that NU-1000/AuNP and NU-1000/PDA/AuNP composites contained ca. 14 and 21 wt% gold, respectively, indicating that the MOF-encapsulated PDA containing amine and OH groups produced more AuNPs possibly due to more efficient reduction of Au^{3+} ions than pristine NU-1000, the effects of which were reflected on their electrical conductivity.[85] N_2-sorption studies showed that although the Brunauer-Emmett-Teller (BET) surface areas of NU-1000/AuNP (1527 m^2/g) and NU-1000/PDA/AuNP (715 m^2/g) composites were lower than that of pristine NU-1000 (2215 m^2/g)[70,84] due to the presence of embedded PDA and AuNPs, they still remained adequately porous while dramatically gaining electrical conductivity. Two-probe current–voltage (*I-V*) measurements revealed that whereas NU-1000, NU-1000/PDA, and PDA/AuNP pellets practically behaved as insulators ($\sigma \leq 10^{-12}$ S/cm), NU-1000/AuNP and NU-1000/PDA/AuNP composites displayed several orders of magnitude higher room-temperature electrical conductivity (σ = 1.2 (±0.1) × 10^{-7} and 5.2 (±0.04) × 10^{-7} S/cm, respectively) possibly due to more efficient charge-hopping and/or tunneling across the framework enabled by the well-distributed AuNPs embedded in the MOF.[84] To our knowledge, the room-temperature conductivities of both NU-1000/AuNP and NU-1000/PDA/AuNP composites are four orders of magnitude higher than that displayed by any other MOF/MNP composites thus far (i.e., AgNC@Rb-CD MOF)[83] while their BET surface areas are also higher than that of many intrinsically conducting 3D porous MOFs.[86–91] Thus, this work presents a novel strategy to convert highly porous but intrinsically insulating MOFs into semiconducting MOF/MNP and MOF/Polymer/MNP composites, which also possess significant porosity.

RESULTS AND DISCUSSION

To demonstrate the possibility of transforming an intrinsically insulating, porous MOF into electrically conducting MOF/MNP and MOF/polymer/MNP composites with sizable porosity and surface areas, we have employed NU-1000 MOF because its large pores and exceptional chemical and structural stabilities are well suited for facile infiltration of dopamine monomers and Au^{3+} ions and subsequent *in situ* oxidative polymerization and reductive AuNP formation. NU-1000 was synthesized by a solvothermal reaction between $ZrOCl_2 \cdot 8H_2O$ and a TBPy ligand according to a literature protocol,[92] and its crystalline structure and phase-purity were confirmed by PXRD analysis. Upon soaking a bright yellow colored activated NU-1000 powder into an aqueous $AuCl_3$ solution (2 mM) overnight, the suspension turned orange, which was washed thoroughly and dried (see Supporting Information (SI) for details). The PXRD profile (Figure 2) of the resulting orange powder not only featured the characteristic NU-1000 peaks ($2\theta \approx$ 2.5, 5.0, 7.5, and 10°), but also characteristic [111] and [200] peaks of metallic AuNPs at $2\theta \approx$ 38 and 45°, respectively,[82] indicating the formation of metallic AuNPs via reduction of infiltrated Au^{3+} ions by the OH groups of the $Zr_6(\mu_3\text{-}O)_4(\mu_3\text{-}OH)_4(OH)_4(H_2O)_4$ nodes, as evident from the IR spectrum of NU-1000 (Figure S1). This observation was consistent with previous reports of metallic AuNP formation via Au^{3+} reduction by MIL-100(Fe)[82] and AgNPs formation via Ag^+ reduction by the hydroxyl groups in Rb-CD MOF.[83]

Recent studies have demonstrated[82] that although pristine MIL-100(Fe) can reduce infiltrated Au^{3+} ions into metallic AuNPs, MOF-embedded organic polymers having electron-donating amine and hydroxyl

groups can reduce Au^{3+} ions more efficiently to produce larger amounts of metallic gold. Therefore, we functionalized the NU-1000 pores with polydopamine via aerobic oxidation of preloaded dopamine monomers by a double-solvent method[93] (see SI for details). Briefly, to a suspension of activated NU-1000 in dry hexane a small amount of aqueous solution of dopamine hydrochloride was added. Hexane's low vapor pressure, poor interfacial tension with water, and weak interaction with the internal surface of NU-1000 facilitated infusion of the monomer into NU-1000 pores and prevented unwanted polymerization on the outer surface of the MOF. Then, an aqueous NH_4OH solution was added to the reaction mixture to neutralize dopamine hydrochloride and trigger oxidative polymerization to polydopamine in the presence of air (O_2). Consequently, the bright yellow colored NU-1000 suspension turned olive indicating the formation of NU-1000/PDA composite, which was washed extensively to remove unreacted dopamine monomers and dried under vacuum. The PXRD profile of the resulting olive powder (Figure 2a) featured the characteristic NU-1000 peaks, indicating that the crystalline structure of the MOF remained intact after PDA formation and that the PDA chains were mostly confined to NU-1000 pores (if amorphous PDA coated the external surfaces of hexagonal rod-shaped NU-1000 crystals, then the crystallinity of the resulting composite would have been severely diminished). Subsequently, the NU-1000/PDA composite was soaked in an aqueous $AuCl_3$ solution (2 mM) and stirred at room temperature for overnight, which led to a distinct color change of the suspension from olive to ochre, indicating the formation of metallic AuNP via the reduction of Au^{3+} ions. The resulting material was collected by centrifugation, washed thoroughly with H_2O and MeOH, and dried under vacuum for subsequent studies. The PXRD profile of the resulting NU-1000/PDA/AuNP composite (Figure 2a) also featured the characteristic peaks of NU-1000 ($2\theta \approx$ 2.5, 5.0, 7.5, and 10°) as well as of metallic AuNPs ($2\theta \approx$ 38 and 45°),[82] confirming the presence of AuNPs in this composite as well. Although a MIL-100(Fe)/PDA composite had been previously used to extract Hg, Pb, and Pd from aqueous solutions of respective salts,[81] this is the first demonstration of AuNP formation from an Au^{3+} solution by a MOF/PDA composite. For control studies, free PDA was prepared by aerobic oxidation of dopamine monomer in the absence of NU-1000, and a PDA/AuNP composite by soaking free PDA into an aqueous $AuCl_3$ solution (2 mM) under the same conditions. According to PXRD analysis (Figure 2a), free PDA was amorphous, whereas PDA/AuNP displayed only the characteristic AuNP peaks confirming the PDA-induced reduction Au^{3+} ions to metallic AuNPs.

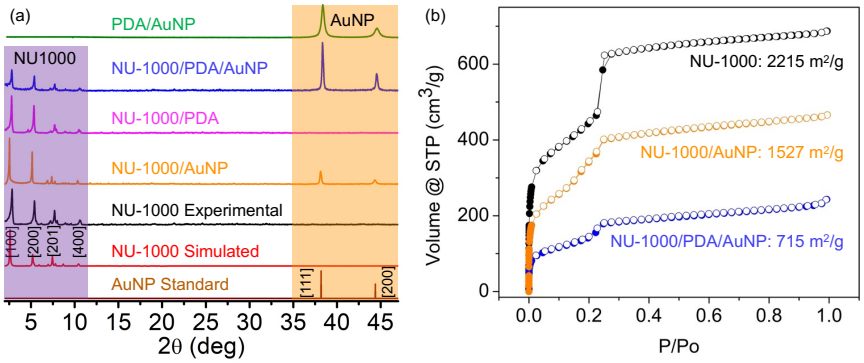

Figure 2. (a) PXRD profiles of NU-1000, AuNP, NU-1000/AuNP, NU-1000/PDA, NU-1000/PDA/AuNP, and PDA/AuNP. (b) N_2 sorption isotherms (77 K) of pristine NU-1000 (black), NU-1000/AuNP (orange), and NU-1000/PDA/AuNP (blue), adsorption: closed circles, desorption: open circles.

N_2-sorption studies (Figure 2b) revealed that compared to highly porous NU-1000 (2215 m^2/g),[70] activated NU-1000/AuNP and NU-1000/PDA/AuNP composites possessed smaller BET surface areas

(1527 and 715 m^2/g, respectively) due to the presence of embedded PDA and AuNPs inside the pores. The smaller surface area of NU-1000/PDA/AuNP than that of NU-1000/AuNP composite can be attributed the presence of both PDA and AuNPs in the former. Notably, the surface area of NU-1000/AuNP was still slightly higher than that of a Ni-carborane (NiCB)-doped NU-1000 (1260 m^2/g), which displayed a similar range of conductivity.[70] Although smaller than pristine MOF's, the surface areas of semiconducting NU-1000/AuNP and NU-1000/PDA/AuNP composites were still larger than most 3D porous MOFs having comparable conductivity,[86–91] suggesting that this could be an effective strategy to create electronic conductivity while preserving sufficient porosity of MOF materials, thus combining two most desired but conflicting features in a single platform.

The FT-IR analysis of NU-1000/PDA and NU-1000/PDA/AuNP composites (Figure S1) showed the characteristic PDA signals at ca. 1600 and 1300 cm^{-1} corresponding to C=C, C=N, and C=N–C bond stretching vibrations, respectively, confirming the presence of PDA in these materials. TGA revealed (Figure S2) that while free PDA gradually decomposed with increasing temperature and completely vanished as CO_2, H_2O, and N-oxides gasses leaving no residual weight at ~600 °C, thermally decomposed PDA/AuNP composite left a constant ~53% residual weight corresponding to metallic Au after complete disappearance of PDA. In contrast, NU-1000, NU-1000/AuNP, NU-1000/PDA, and NU-1000/PDA/AuNP displayed small initial weight loss due to solvent loss (~10 % up to 100 °C), followed by a stable plateau before decomposing at higher temperature (≥ 400 °C) leading to a sharp weight loss. The residual weights of these thermally decomposed materials—NU-1000 (~33 %), NU-1000/AuNP (~47 %), NU-1000/PDA (~28 %), and NU-1000/PDA/AuNP (~50 %)—accounted for indestructible ZrO_2 and Au (the MOF-embedded PDA should also vanish completely), which provided valuable insights into the amounts of MOF-embedded PDA and AuNP in each composite. Based on the molecular formula ($Zr_6C_{88}H_{60}O_{32}$) and formula weight (2176.74) of NU-1000,[92] a fully pyrolyzed NU-1000 formula unit can produce six ZrO_2 molecules (FW: 123.3, total weight: 739.8), which accounted for ~33% weight of the pristine MOF. In other words, 33% residual weight corresponding to remaining ZrO_2 in thermally decomposed NU-1000 corresponds to 100 % of original NU-1000. Therefore, the higher residual weight of fully decomposed NU-1000/AuNP composite (~47 %) suggested that it contained ~14 wt% of embedded AuNPs. On the other hand, the smaller residual weight of thermally decomposed NU-10000/PDA composite (~28 %), which stemmed entirely from ZrO_2 (the embedded PDA vanished), corresponded to 85 wt% of NU-1000, leaving ~15 wt% of embedded PDA in this composite. Thus, the residual weight of fully decomposed NU-1000/PDA/AuNP (~50 %) than NU-1000/PDA (~28 %) suggested that the difference (~22 wt%) stemmed from the embedded AuNPs in the former. Thus, the AuNPs content in NU-1000/PDA/AuNP (~22 wt%) was ~1.5 times greater than in NU-1000/AuNP (~14 wt%) possibly due to the fact that the electron-donating catechol and amine groups of embedded PDA led to more efficient reduction of infiltrated Au^{3+} ions to AuNPs than the Zr^{4+}-bound OH groups of pristine NU-1000.

The presence of embedded PDA and AuNPs in NU-1000/AuNP and NU-1000/PDA/AuNP composites was further confirmed by SEM and STEM-EDX analyses (Figure 3). The SEM images (Figure 3a–d, left) revealed hexagonal rod-shaped crystals of pristine NU-1000, which remained largely intact in NU-1000/AuNP, NU-1000/PDA, and NU-1000/PDA/AuNP composites. No polymer brush protruding out of the smooth surfaces and sharp, well-defined edges of NU-1000 crystals was observed, suggesting that the *in situ* generated PDA was mostly confined to the MOF pores instead of growing on the outer surface. The STEM-EDX analysis (Figure 3a–d, colored panels) revealed that in addition to signature elements of the host MOF (Zr, C, and O), NU-1000/AuNP composite contained Au; NU-1000/PDA featured N, the

signature element of PDA; and NU-1000/PDA/AuNP contained both N and Au, confirming the coexistence and uniform distribution of each component of respective composites. Furthermore, cross-sectional SEM and STEM-EDX analysis (Figure 3e–h) of 100 nm thick slices of NU-1000, NU-1000/AuNP, NU-1000/PDA, and NU-1000/PDA/AuNP embedded in epoxy resin revealed uniform distribution of the signature elements of each component inside the well-defined hexagonal cross-sections of NU-1000 crystals, i.e., Zr, C, and O in pristine NU-1000; Zr, C, O, and N in NU-1000/PDA; and Zr, C, O, N, and Au in NU-1000/PDA/AuNP, confirming the presence of the PDA and AuNPs inside the MOF. Back-scattered and secondary electron SEM image of NU-1000/PDA/AuNP composite (Figure S3) further confirmed the presence of AuNPs embedded underneath the MOF surface.

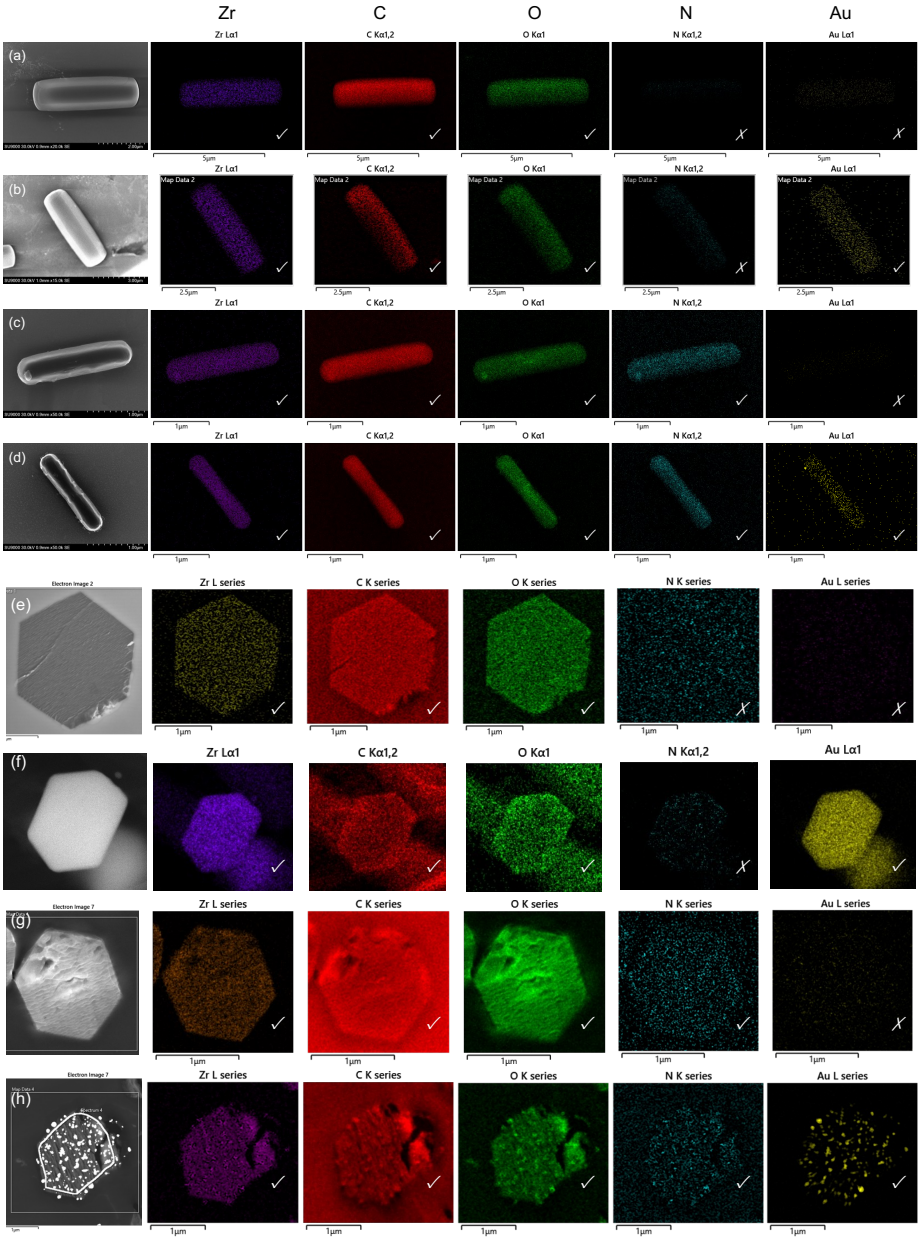

Figure 3. (a–d) The SEM images (left) and color-coded STEM-EDX elemental mapping (right) of (a) pristine NU-1000, (b) NU-1000/AuNP, (c) NU-1000/PDA, and (d) NU-1000/PDA/AuNP. (e–h) Cross-sectional SEM images (left) and color-coded STEM-EDX elemental mapping (right) of (e) pristine NU-1000, (f) NU-1000/AuNP, (g) NU-1000/PDA, and (h) NU-1000/PDA/AuNP.

Finally, room-temperature electrical conductivities of NU-1000, NU-1000/AuNP, NU-1000/PDA, and NU-1000/PDA/Au were determined by two-probe *I–V* measurements (Figure 4a and S4) performed on pressed pellets of respective materials sandwiched between two stainless steel electrodes surrounded by a snug-fit Teflon tube. Since NU-1000 lacks well-defined through-bond and/or through π-stack conduction pathways[4–7] it relies on relatively less efficient redox-hopping between spatially well-separated ligands. Therefore, although horizontally and vertically oriented NU-1000 thin films displayed modest anisotropic conductivity (10^{-9} and 10^{-7} S/cm, respectively) due to more efficient redox-hopping along the c-axis,[84] NU-1000 and NU-1000/PDA pellets consisting of randomly oriented MOF crystallites practically acted as insulators without showing any meaningful conductivity ($\leq 10^{-12}$ S/cm, Figure S4). In contrast, NU-1000/AuNP and NU-1000/PDA/AuNP pellets displayed several orders of higher room temperature electrical conductivity—1.2 (±0.1) × 10^{-7} and 5.2 (±0.04) × 10^{-7} S/cm, respectively—which was attributed to more efficient charge hopping and/or tunnelling[83] facilitated by the *in-situ* generated AuNPs located inside the MOF. The slightly higher conductivity of NU-1000/PDA/AuNP than NU-1000/AuNP could be attributed to higher AuNP content in the former. In contrast, the MOF-free PDA/AuNP composite displayed negligible conductivity (3.2 × 10^{-11} S/cm, Figure S4), demonstrating that randomly distributed AuNPs embedded in amorphous PDA matrix did not support efficient charge hopping. On the other hand, crystalline NU-1000 enabled more orderly distribution of AuNPs inside its cavities, leading to more efficient long-range charge hopping and higher electrical conductivities of NU-1000/AuNP and NU-1000/PDA/AuNP composites, demonstrating a distinct benefit of the crystalline MOF over amorphous PDA. While the conductivities of NU-1000/AuNP and NU-1000/PDA/AuNP composites are comparable to that of NiCB@NU-1000,[70] NU-1000/AuNP possesses larger surface area than NiCB@NU-1000 (1527 vs. 1260 m^2/g), demonstrating that AuNPs can be installed to successfully convert intrinsically insulating porous MOFs into electrically conducting composite while retaining sizeable porosity. Furthermore, the room-temperature conductivities of NU-1000/AuNP and NU-1000/PDA/AuNP composites are 10^4 times higher than that displayed by AgNP@Rb-CD without any light and/or thermal induction,[83] to our knowledge, the only other electrically conducting MOF/MNPs composite reported to date. In this context, it is also important to note that the bulk conductivity values of MOFs pellets are usually 1–3 orders of magnitude smaller than the values measured with single-crystals and specifically oriented MOF films due to the contributions of grain boundary resistance and random distribution of MOF crystallites in the pellets. Finally, the thermal activation energies of NU-1000/AuNP (E_a = 0.24 eV) and NU-1000/PDA/AuNP (E_a = 0.12 eV) composites were determined from the Arrhenius plots (Figure 4b and c) of respective temperature-dependent electrical conductivity values, which confirmed their semiconducting nature. Thus, an intrinsically insulating NU-1000 MOF was successfully transformed into semiconducting NU-1000/AuNP and NU-1000/PDA/AuNP composites while also preserving significant porosity and surface area of the host MOF.

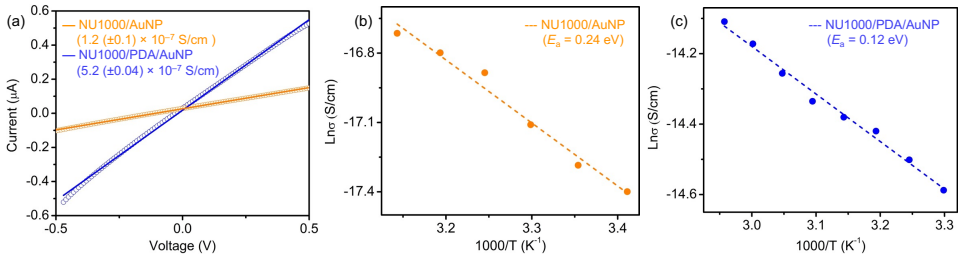

Figure 4. (a) Representative *I-V* plots of NU-1000/AuNP (orange) and NU-1000/PDA/AuNP (blue). Arrhenius plots of temperature-dependent conductivity of (b) NU-1000/AuNP (orange) and (c) NU-1000/PDA/AuNP (blue) revealing their respective activation energies.

CONCLUSIONS

The foregoing studies demonstrated that while pristine NU-1000 itself could reduce the infiltrated Au^{3+} ions to metallic AuNPs forming NU-1000/AuNP composite, a NU-1000/PDA composite obtained by oxidative polymerization of preloaded dopamine monomers yielded NU-1000/PDA/AuNP composite containing a higher AuNP content due to the better reducing capacity of electron-donating PDA polymer. The SEM and STEM-EDX analyses revealed the coexistence and uniform distribution of signature elements of each component of respective composites, confirming the presence of PDA and AuNPs inside NU-1000 pores. Although NU-1000/AuNP and NU-1000/PDA/AuNP composites became less porous than pristine NU-1000, they still retained sizeable porosity (BET surface areas 1527 and 715 m^2/g, respectively), while gaining significant electrical conductivity (~10^{-7} S/cm), which pristine NU-1000 lacked. Notably, the bulk electrical conductivities of NU-1000/AuNP and NU-1000/PDA/AuNP composites are on par with that of NiCB-doped NU-1000 films and 10^4 times higher than that of the only other MOF/MNP composite (Rb-CD/AgNP) with a measurable conductivity reported to date. The markedly higher conductivity of NU-1000/AuNP and NU-1000/PDA/AuNP composites is attributed to more efficient charge hopping or tunneling through well-dispersed and organized AuNPs embedded inside crystalline NU-1000 matrix, which practically insulating NU-1000, NU-1000/PDA, and PDA/AuNP lacked. Thus, this work presents an effective novel strategy to convert porous but non/poor conducting MOFs into electrically conducting MOF/MNP and MOF/polymer/MNP composites with sizeable porosity, which will help expand their utility in modern electronics and energy technologies.

ASSOCIATED CONTENT

Supporting Information

Supporting Information is available free of charge at https://.... Experimental details and additional data (PDF).

AUTHOR INFORMATION

Corresponding Author

Sourav Saha — Department of Chemistry, Clemson University, Clemson, South Carolina 29634, United States; orcid.org/0000-0001-6610-4820;

Email: souravs@clemson.edu

Authors

Monica Gordillo — Department of Chemistry, Clemson University, Clemson, South Carolina 29634, United States; orcid.org/0000-0002-6326-421X

Paola A. Benavides — Department of Chemistry, Clemson University, Clemson, South Carolina 29634, United States; orcid.org/0000-0002-1701-5036

Kaikai Ma — Department of Chemistry, Northwestern University, 2145 Sheridan Road, Evanston, IL 60208, United States

Author Contributions

The manuscript was written through contributions of all authors. All authors approved the final version of the manuscript.

Notes

The authors declare no competing financial interest.

ACKNOWLEDGEMENTS

This work was supported by the National Science Foundation (award no. DMR-1809092). K.M. acknowledges the financial support from the Army Research Office (W911NF1910340). We thank Prof. Omar K. Farha of Northwestern University for kindly providing us with a batch of NU-1000 MOF used in our preliminary studies.

REFERENCES

(1) Zhou, H. C.; Long, J. R.; Yaghi, O. M. Introduction to metal–organic frameworks. *Chem. Rev.* **2012**, *112*, 673–674.

(2) Furukawa, H.; Cordova, K. E.; O'Keeffe, M.; Yaghi, O. M. The Chemistry and Applications of Metal-Organic Frameworks. *Science* **2013**, *341*, 974–986.

(3) Jacoby, M. Conductive MOFs: Surprising Charge Transport Property Could Lead to New Applications. *C&EN* **2021**, *99* (43), 30–34.

(4) Sun, L.; Campbell, M. G.; Dincă, M. Electrically Conductive Porous Metal–Organic Frameworks. *Angew. Chem. Int. Ed.* **2016**, *55*, 3566–3579.

(5) Leong, C. F.; Usov, P. M.; D'Alessandro, D. M. Intrinsically Conducting Metal-Organic Frameworks. *MRS Bull.* **2016**, *41*, 858–864.

(6) Ko, M.; Mendecki, L.; Mirica, K. A. Conductive Two-Dimensional Metal−Organic Frameworks as Multifunctional Materials. *Chem. Commun*. **2018**, *54*, 7873−7891.

(7) Xie, L. S.; Skorupskii, G.; Dincă, M. Electrically Conductive Metal–Organic Frameworks. *Chem. Rev.* **2020**, *120*, 8536–8580.

(8) Gordillo, M. A.; Saha, S. Strategies to Improve Electrical and Ionic Conductivities of Metal–Organic Frameworks. *Comments on Inorg. Chem.* **2020**, *40*, 86–106.

(9) Johnson, E.; Ilic, S.; Morris, A. J. Design Strategies for Enhanced Conductivity in Metal-Organic Frameworks. *ACS Cent. Sci*. **2021**, *7*, 445–453.

(10) Wang, M.; Dong, R.; Feng, X. Two-Dimensional Conjugated Metal–Organic Frameworks (2D c-MOFs): Chemistry and Function for MOFtronics. *Chem. Soc. Rev.* **2021**, *50*, 2764–2793.

(11) Stavila, V.; Talin, A. A.; Allendorf, M. D. MOF-based Electronic and Optoelectronic Devices. *Chem. Soc. Rev.* **2014**, *43*, 5994-6010.

(12) Dolgopolova, E. A.; Shustova, N. B. Metal-Organic Frameworks Photophysics: Optoelectronic Devices, Photoswitches, Sensor, and Photocatalysts. *MRS Bull.* **2016**, *41*, 890–896.

(13) Maza, W. A.; Haring, A. J.; Ahrenholtz, S. R.; Epley, C. C.; Lin, S. Y.; Morris, A. J. Ruthenium (II)-Polypyridyl Zirconium (IV) Metal–Organic Frameworks as a New Class of Sensitized Solar Cells. *Chem. Sci.* **2016**, *7*, 719–727.

(14) Stassen, I.; Burtch, N.; Talin, A.; Falcaro, P.; Allendorf, M.; Ameloot, R. An Updated Roadmap for the Integration of Metal–Organic Frameworks with Electronic Devices and Chemical Sensors. *Chem. Soc. Rev.* **2017**, *46*, 3185–3241.

(15) Wang, H.; Zhu, Q.-L.; Zou, R.; Xu, Q. Metal-Organic Frameworks for Energy Applications. *Chem* **2017**, *2*, 52−80.

(16) Gordillo, M. A.; Panda, D. K.; Saha, S. Efficient MOF-Sensitized Solar Cells Featuring Solvothermally Grown [100]-Oriented Pillared Porphyrin Framework-11 Films on ZnO-FTO Surfaces. *ACS Appl. Mater. Interfaces* **2019**, *11*, 3196–3206.

(17) Allendorf, M.; Dong, R.; Feng, X.; Kaskel, S.; Matoza, D.; Stavila, V. Electronic Devices Using Open Framework Materials. *Chem. Rev*. **2020**, *120*, 8581–8640.

(18) Zhang, Z.; Awaga, K.; Redox-Active Metal-Organic Frameworks as Electrode Materials for Batteries. *MRS Bull.* **2016**, 41, 883–889.

(19) Nam, K. W.; Park, S. S.; dos Reis, R.; Dravid, V. P.; Kim, H.; Mirkin, C. A.; Stoddart, J. F. Conductive 2D Metal-Organic Framework for High-Performance Cathodes in Aqueous Rechargeable Zinc Batteries. *Nat. Commun*. **2019**, *10*, 4948.

(20) Wen, X.; Zhang, Q.; Guan, J. Applications of Metal–Organic Framework-Derived Materials in Fuel Cells and Metal-Air Batteries. *Coord. Chem. Rev*. **2020**, *409*, 213214.

(21) Wang, L.; Han, Y. Z.; Feng, X.; Zhou, J. W.; Qi, P. F.; Wang, B., Metal–Organic Frameworks for Energy Storage: Batteries and Supercapacitors. *Coord. Chem. Rev.* **2016,** *307*, 361–381.

(22) Xu, G.; Nie, P.; Dou, H.; Ding, B.; Li, L.; Zhang, X. Exploring Metal Organic Frameworks for Energy Storage in Batteries and Supercapacitors. *Mater. Today* **2017**, 20, 191–209.

(23) Sheberla, D.; Bachman, J. C.; Elias, J. S.; Sun, C.-J.; Shao-Horn, Y.; Dincă, M. Conductive MOF Electrodes for Stable Supercapacitors with High Areal Capacitance. *Nat. Mater.* **2017**, *16*, 220−224.

(24) Li, W.-H.; Ding, K.; Tian, H.-R.; Yao, M.-S.; Nath, B.; Deng, W.-H.; Wang, Y.; Xu, G. Conductive Metal-Organic Framework Nanowire Array Electrodes for High-Performance Solid-State Supercapacitors. *Adv. Funct.* Mater. **2017**, *27*, 1702067.

(25) Wu, H.; Zhang, W.; Kandambeth, S.; Shekhah, O.; Eddaoudi, M.; Alshareef, H. N. Conductive Metal-Organic Frameworks Selectively Grown on Laser-Scribed Graphene for Electrochemical Microsupercapacitors. *Adv. Energy Mater*. **2019**, *9*, 1900482.

(26) Wu, G.; Huang, J.; Zang, Y.; He, J.; Xu, G. Porous Field-Effect Transistors Based on a Semiconductive Metal−Organic Framework. *J. Am. Chem. Soc*. **2017**, *139*, 1360−1363.

(27) Wang, B.; Luo, Y.; Liu, B.; Duan, G. Field-Effect Transistor Based on an in situ Grown Metal−Organic Framework Film as a Liquid-Gated Sensing Device. *ACS Appl. Mater. Interfaces* **2019**, *11*, 35935−35940.

(28) Campbell, M. G.; Sheberla, D.; Liu, S. F.; Swager, T. M.; Dincă, M. Cu_3(Hexaiminotriphenylene)$_2$: An Electrically Conductive 2D Metal-Organic Framework for Chemiresistive Sensing. *Angew. Chem. Int. Ed*. **2015**, *54*, 4349−4352.

(29) Campbell, M. G.; Liu, S. F.; Swager, T. M.; Dincă, M. Chemiresistive Sensor Arrays from Conductive 2D Metal-Organic Frameworks. *J. Am. Chem. Soc.* **2015**, *137*, 13780−13783.

(30) Yao, M.-S.; Lv, X.-J.; Fu, Z.-H.; Li, W.-H.; Deng, W.-H.; Wu, G.-D.; Xu, G. Layer-by-Layer Assembled Conductive Metal-Organic Framework Nanofilms for Room-Temperature Chemiresistive Sensing. *Angew. Chem. Int. Ed*. **2017**, *56*, 16510−16514.

(31) Rubio-Gimenez, V.; Almora-Barrios, N.; Escorcia-Ariza, G.; Galbiati, M.; Sessolo, M.; Tatay, S.; Marti-Gastaldo, C. Origin of the Chemiresistive Response of Ultrathin Films of Conductive Metal-Organic Frameworks. *Angew. Chem. Int. Ed*. **2018**, *57*, 15086−15090.

(32) Aubrey, M. L.; Kapelewski, M. T.; Melville, J. F.; Oktawiec, J.; Presti, D.; Gagliardi, L.; Long, J. R. Chemiresistive Detection of Gaseous Hydrocarbons and Interrogation of Charge Transport in Cu[Ni(2,3-Pyrazinedithiolate)$_2$] by Gas Adsorption. *J. Am. Chem. Soc.* **2019**, *141*, 5005−5013.

(33) Yao, M.-S.; Zheng, J.-J.; Wu, A.-Q.; Xu, G.; Nagarkar, S. S.; Zhang, G.; Tsujimoto, M.; Sakaki, S.; Horike, S.; Otake, K.; Kitagawa, S. A Dual-Ligand Porous Coordination Polymer Chemiresistor with Modulated Conductivity and Porosity. *Angew. Chem. Int. Ed*. **2020**, *59*, 172−176.

(34) Koo, W.-T.; Jang, J.-S.; Kim, I.-D. Metal-Organic Frameworks for Chemiresistive Sensors. *Chem* **2019**, *5*, 1938−1963.

(35) Clough, A. J.; Yoo, J. W.; Mecklenburg, M. H.; Marinescu, S. C. Two-Dimensional Metal−Organic Surfaces for Efficient Hydrogen Evolution from Water. *J. Am. Chem. Soc*. **2015**, *137*, 118−121.

(36) Miner, E. M.; Fukushima, T.; Sheberla, D.; Sun, L.; Surendranath, Y.; Dincă, M. Electrochemical Oxygen Reduction Catalysed by Ni_3(Hexaiminotriphenylene)$_2$. *Nat. Commun*. **2016**, *7*, 10942.

(37) Lin, S.; Pineda-Galvan, Y.; Maza, W. A.; Epley, C. C.; Zhu, J.; Kessinger, M. C.; Pushkar, Y.; Morris, A. J. Electrochemical Water Oxidation by a Catalyst-Modified Metal–Organic Framework Thin Film. *ChemSusChem* **2017**, 10, 514–522.

(38) Downes, C. A.; Marinescu, S. C. Electrocatalytic Metal−Organic Frameworks for Energy Applications. *ChemSusChem* **2017**, *10*, 4374−4392.

(39) Downes, C. A.; Clough, A. J.; Chen, K.; Yoo, J. W.; Marinescu, S. C. Evaluation of the H_2 Evolving Activity of Benzenehexathiolate Coordination Frameworks and the Effect of Film Thickness on H_2 Production. *ACS Appl. Mater. Interfaces* **2018**, *10*, 1719−1727.

(40) Miner, E. M.; Wang, L.; Dincă, M. Modular O_2 Electroreduction Activity in Triphenylene-Based Metal-Organic Frameworks. *Chem. Sci*. **2018**, *9*, 6286−6291.

(41) Yi, J. D.; Shi, D. H.; Xie, R.; Yin, Q.; Zhang, M. D.; Wu, Q.; Chai, G. L.; Huang, Y. B.; Cao, R. Conductive Two-Dimensional Phthalocyanine-based Metal–Organic Framework Nanosheets for Efficient Electroreduction of CO_2. *Angew. Chem. Int. Ed.* **2021**, *60* 17108–17114.

(42) He, Y.; Zhou, W.; Qian, G.; Chen, B., Methane storage in metal–organic frameworks, *Chem. Soc. Rev.* **2014**, *43*, 5657–5678.

(43) Sumida, K.; Rogow, D. L.; Mason, J. A.; McDonald, T. M.; Bloch, E. D.; Herm, Z. R.; Bae, T.-H.; Long, J. R. Carbon Dioxide Capture in Metal-Organic Frameworks. *Chem. Rev.* **2012**, *112*, 724–781.

(44) Wu, H.; Gong, Q.; Olson, D. H.; Li, J. Commensurate Adsorption of Hydrocarbons and Alcohols in Microporous Metal Organic Frameworks. *Chem. Rev.* **2012**, *112*, 836–868.

(45) Suh, M. P.; Park, H. J.; Prasad, T. K.; Lim, D.-W. Hydrogen Storage in Metal–Organic Frameworks. *Chem. Rev.* **2012**, *112*, 782–835.

(46) Getman, R. B.; Bae, Y.-S.; Wilmer, C. E.; Snurr, R. Q. Review and Analysis of Molecular Simulations of Methane, Hydrogen, and Acetylene Storage in Metal–Organic Frameworks. *Chem. Rev.* **2012**, *112*, 703–723.

(47) Li, J.-R.; Sculley, J.; Zhou, H.-C. Metal–Organic Frameworks for Separations. *Chem. Rev.* **2012**, *112*, 869–932.

(48) Herm, Z. R.; Bloch, E. D.; Long, J. R. Hydrocarbon Separations in Metal-Organic Frameworks. *Chem. Mater.* **2014**, *26*, 323−338.

(49) Adil, K.; Belmabkhout, Y.; Pillai, R. S.; Cadiau, A.; Bhatt, P. M.; Assen, A. H.; Maurin, G.; Eddaoudi, M. Gas/Vapour Separation Using Ultra-Microporous Metal−Organic Frameworks: Insights into the Structure/Separation Relationship. *Chem. Soc. Rev.* **2017**, *46*, 3402−3430.

(50) Horcajada, P.; Gref, R.; Baati, T.; Allan, P. K.; Maurin, G.; Couvreur, P.; Férey, G.; Morris, R. E.; Serre, C. Metal–organic frameworks in biomedicine. *Chem. Rev.* **2012**, *112*, 1232–1268.

(51) Ma, L.; Abney, C.; Lin, W. Enantioselective catalysis with homochiral metal–organic frameworks. *Chem. Soc. Rev.* **2009**, *38*, 1248–1256.

(52) Lee, J. Y.; Farha, O. K.; Roberts, J.; Scheidt, K. A.; Nguyen, S. B. T.; Hupp, J. T. Metal–organic framework materials as catalysts. *Chem. Soc. Rev.* **2009**, *38*, 1450–1459.

(53) Liu, J.; Chen, L.; Cui, H.; Zhang, J.; Zhang, L.; Su, C.-Y. Application of metal–organic frameworks in heterogeneous supramolecular catalysis. *Chem. Soc. Rev.* **2014**, *43*, 6011–6061.

(54) Bavykina, A.; Kolobov, N.; Khan, I. S.; Bau, J. A.; Ramirez, A.; Gascon, J. Metal–Organic Frameworks in Heterogeneous Catalysis: Recent Progress, New Trends, and Future Perspectives. *Chem. Rev.* **2020**, *120*, 8468–8535.

(55) Zhang, W.; Nafady, A.; Shan, C.; Wojtas, L.; Chen, Y.-S.; Cheng, Q.; Zhang, X. P.; Ma, S. Functional Porphyrinic Metal-Organic Framework as a New Class of Heterogeneous Halogen Bond Donor Catalyst. *Angew Chem. Int. Ed*. **2021**, *60*, 24312–24317.

(56) Liao, Y.; Sheridan, T.; Liu, J.; Farha, O. K.; Hupp, J. T. Product Inhibition and the Catalytic Destruction of a Nerve Agent Simulant by Zirconium-Based Metal–Organic Frameworks. *ACS Appl. Mater. Interfaces* **2021**, *13*, 30565–30575.

(57) Mian, M. R.; Chen, H.; Cao, R.; Kirlikovali, K. O.; Snurr, R. Q.; Islamoblu, T.; Farha, O. K. Insights into Catalytic Hydrolysis of Organophosphonates at M–OH Sites of Azolate-Based Metal Organic Frameworks. *J. Am. Chem. Soc.,* **2021**, *143*, 9893–9900.

(58) Kreno, L. E.; Leong, K.; Farha, O. K.; Allendorf, M.; Van Duyne, R. P.; Hupp, J. T., Metal–Organic Framework Materials as Chemical Sensors. *Chem. Rev.* **2012**, *112*, 1105–1125.

(59) Hu, Z.; Deibert, B. J.; Li, J. Luminescent metal–organic frameworks for chemical sensing and explosive detection. *Chem. Soc. Rev.* **2014**, *43*, 5815–5840.

(60) Barea, E.; Montoro, C.; Navarro, J. A. R. Toxic gas removal — metal–organic frameworks for the capture and degradation of toxic gases and vapours. *Chem. Soc. Rev.* **2014**, *43*, 5419–5430.

(61) Dolgopolova, E. A.; Rice, A. M., Martin, C. R.; Shustova, N. B. Photochemistry and photophysics of MOFs: steps towards MOF-based sensing enhancements. *Chem. Soc. Rev.* **2018**, *47*, 4710–4728.

(62) Allendorf, M. A.; Foster, M. E.; Léonard, F.; Stavila, V.; Feng, P. L.; Doty, F. P.; Leong, K.; Ma, E. Y.; Johnston, S. R.; Talin, A. A. Guest-Induced Emergent Properties in Metal−Organic Frameworks. *J. Phys. Chem. Lett.* **2015**, *6*, 1182–1195.

(63) Ullman, A. M.; Brown, J. W.; Foster, M. E.; Léonard, F.; Leong, K.; Stavila, V.; Allendorf, M. D. Transforming MOFs for Energy Applications Using Guest@MOF Concept. *Inorg. Chem.* **2016**, *55*, 7233–7249.

(64) Allendorf, M.; Medishetty, R.; Fischer, R. A. Guest Molecule as a Design Element for Metal-Organic Frameworks. *MRS Bull.* **2016**, *41*, 865–869.

(65) Talin, A. A.; Centrone, A.; Ford, A. C.; Foster, M. E.; Stavila, V.; Haney, P.; Kinney, R. A.; Szalai, V.; Gabaly, F. E.; Yoon, H. P.; Léonard, F.; Allendorf, M. D.; Tunable Electrical Conductivity in Metal-Organic Framework Thin-Film Devices. *Science* **2014**, *343*, 66–69.

(66) Guo, Z.; Panda, D. K.; Maity, K.; Lindsey, D.; Parker, T. G.; Albrecht-Schmitt, T. E.; Barreda-Esparza, J. L.; Xiong, P.; Zhou, W.; Saha, S., Modulating electrical conductivity of metal–organic framework films with intercalated guest π-systems. *J. Mater. Chem. C* **2016**, *4*, 894–899.

(67) Guo, Z.; Panda, D. K.; Gordillo, M. A; Khatun, A.; Wu, H.; Zhou, W.; Saha, S. Lowering Band Gap of an Electroactive Metal–Organic Framework via Complementary Guest Intercalation. *ACS Appl. Mater. Interfaces* **2017**, *9*, 32413–32417.

(68) Gordillo, M. A.; Benavides, P. A.; Panda, D. K.; Saha, S. Advent of Electrically Conducting Double-Helical Metal–Organic Frameworks Featuring Butterfly-Shaped Electron Rich π-Extended Tetrathiafulvalene Ligands. *ACS Appl. Mater. Interfaces* **2020**, *12*, 12955–12961.

(69) Goswami, S.; Ray, D.; Otake, K.; Kung, C.-W.; Garibay, S. J.; Islamoglu, T.; Atilgan, A.; Cui, Y.; Cramer, C. J.; Farha, O. K.; Hupp, J. T. A Porous, Electrically Conductive Hexa-Zirconium(IV) Metal−Organic Framework. *Chem. Sci*. **2018**, *9*, 4477−4482.

(70) Kung, C.-W.; Otake, K.; Buru, C. T.; Goswami, S.; Cui, Y.; Hupp, J. T.; Spokoyny, A. M.; Farha, O. K. Increased Electrical Conductivity in a Mesoporous Metal−Organic Framework Featuring Metallacarboranes Guests. *J. Am. Chem. Soc*. **2018**, *140*, 3871−3875.

(71) Le Ouay, B.; Kitagawa, S.; Uemura, T. Opening of an Accessible Microporosity in an Otherwise Nonporous Metal–Organic Framework by Polymeric Guests. *J. Am. Chem. Soc.* **2017**, *139*, 7886−7892.

(72) Peng, L.; Yang, S.; Jawahery, S.; Moosavi, S. M.; Huckaba, A. J.; Asgari, M.; Oveisi, E.; Nazeeruddin, M. K.; Smit, B.; Queen, W. L. Preserving Porosity of Mesoporous Metal-Organic Frameworks through the Introduction of Polymer Guests. *J. Am. Chem. Soc.* **2019**, *141*, 12397−12405.

(73) Yang, S.; Peng, L.; Sun, D.; Asgari, M.; Oveisi, E.; Trukhina, O.; Bulut, S.; Jamali, A.; Queen, W. L. A new post-synthetic polymerization strategy makes metal-organic frameworks more stable. *Chem. Sci.* **2019**, *10*, 4542–4549.

(74) Yang, S.; Karve, V. V.; Justin, A.; Kochetygov, I.; Espín, J.; Asgari, M.; Trukhina, O.; Sun, D. T.; Peng, L.; Queen, W. L. Enhancing MOF performance through the introduction of polymer guests. *Coord. Chem. Rev.* **2021**, *427*, 213525.

(75) Le Ouay, B.; Boudot, M.; Kitao, T.; Yanagida, T.; Kitagawa, S.; Uemura, T. Nanostructuration of PEDOT in Porous Coordination Polymers for Tunable Porosity and Conductivity. *J. Am. Chem. Soc.* **2016**, *138*, 10088−10091.

(76) MacLean, M. W. A.; Kiato, T.; Suga, T.; Mizuno, M.; Seki, S.; Uemura, T.; Kitagawa, S. Unraveling Inter- and Intrachain Electronics in Polythiophene Assemblies Mediated by Coordination Nanospaces. *Angew. Chem. Int. Ed*. **2016**, *55*, 708−713.

(77) Dhara, B.; Nagarkar, S. S.; Kumar, J.; Kumar, V.; Jha, P. K.; Ghosh, S. K.; Nair, S.; Ballav, N. Increase in Electrical Conductivity of MOF to Billion-Fold upon Filling the Nanochannels with Conducting Polymer. *J. Phys. Chem. Lett.* **2016**, *7*, 2945−2950.

(78) Wang, T. C.; Hod, I.; Audu, C. O.; Vermeulen, N. A.; Nguyen, S. T.; Farha, O. K.; Hupp, J. T. Rendering High Surface Area, Mesoporous Metal–Organic Frameworks Electronically Conductive. *ACS Appl. Mater, Interfaces* **2017,** *9*, 12584–12591.

(79) Jadhav, A.; Gupta, K.; Ninawe, P.; Ballav, N. Imparting Multifunctionality by Utilizing Biporosity in a Zirconium-Based Metal–Organic Framework. *Angew. Chem. Int. Ed.* **2020**, ***132***, 2235–2239.

(80) Khatun, A.; Yadav, A.; Zhang, S.; Saha, S. Transforming an insulating metal–organic framework into electrically conducting metal–organic framework⊃conducting polymer composites. *Mater. Today Chem*. **2022**, *24*, 100981.

(81) Sun, D. T.; Peng, L.; Reeder, W. S.; Moosavi, S. M.; Tiana, D.; Britt, D. K.; Oveisi, E.; Queen, W. L. Rapid, Selective Heavy Metal Removal from Water by a Metal-Organic Framework/Polydopamine Composite. *ACS Cent. Sci*. **2018**, *4*, 349−356.

(82) Sun, D. T.; Gasilova, N.; Yang, S.; Oveisi, E.; Queen, W. L. Rapid, Selective Extraction of Trace Amounts of Gold from Complex Water Mixtures with a MOF/Polymer Composite. *J. Am. Chem. Soc.* **2018**, *140*, 16697–10703.

(83) Han, S. B.; Warren, S. C.; Yoon, S. M.; Malliakas, C. D.; Hou, X. L.; Wei, Y. H.; Kanatzidis, M. G.; Grzybowski, B. A. Tunneling Electrical Connection to the Interior of Metal Organic Frameworks. *J. Am. Chem. Soc.* **2015**, *137*, 8169–8175.

(84) Goswami, S.; Hod, I.; Duan, J. D.; Kung, C.-W.; Rimoldi, M.; Malliakas, C. D.; Palmer, R. H.; Farha, O. K.; Hupp, J. T. Anisotropic Redox Conductivity within a Metal−Organic Framework. *J. Am. Chem. Soc*. **2019**, *141*, 17696−17702.

(85) Maity, K.; Panda, D. K.; Lochner, E.; Saha, S. Fluoride-Induced Reduction of Ag(I) Cation Leading to Formation of Silver Mirrors and Luminescent Ag-Nanoparticles. *J. Am. Chem. Soc.* **2015**, *137*, 2812–2815.

(86) Park, S. S.; Hontz, E. R.; Sun, L.; Hendon, C. H.; Walsh, A.; Van Voorhis, T.; Dincă, M., Cation-Dependent Intrinsic Electrical Conductivity in Isostructural Tetrathiafulvalene-Based Microporous Metal–Organic Frameworks. *J. Am. Chem. Soc.* **2015**, *137*, 1774–1777.

(87) Xie, L. S.; Sun, L.; Wan, R.; Park, S. S.; DeGayner, J. A.; Hendon, C. H.; Dincă, M. Tunable Mixed-Valence Doping toward Record Electrical Conductivity in a Three-Dimensional Metal−Organic Framework. *J. Am. Chem. Soc*. **2018**, *140*, 7411−7414.

(88) Skorupskii, G.; Dincă, M. Electrical Conductivity in a Porous, Cubic Rare-Earth Catecholate. *J. Am. Chem. Soc.* **2020**, *142*, 6920–6924.

(89) Chen, G.; Gee, L. B.; Xu, W.; Zhu, Y.; Lezama-Pacheco, J. S.; Huang, Z.; Li, Z.; Babicz Jr., J. T.; Choudhury, S.; Chang, T.-H.; Reed, E.; Solomon, E. I.; Bao, Z. Valence-Dependent Electrical Conductivity in a 3D Tetrahydroxyquinone-Based Metal–Organic Framework. *J. Am. Chem. Soc.* **2020**, *142*, 21243–21248.

(90) Yadav, A.; Panda, D. K.; Zhang, S.; Zhou, W.; Saha, S. Electrically Conductive 3D Metal–Organic Framework Featuring π-Acidic Hexaazatriphenylene Hexacarbonitrile Ligands with Anion–π Interaction and Efficient Charge Transport Capabilities. *ACS Appl. Mater. Interfaces* **2020**, 12, 40613–40619.

(91) Zhang, S.; Panda, D. K.; Yadav. A.; Zhou, W.; Saha, S. Effects of Intervalence Charge Transfer Interaction between π-Stacked Mixed Valent Tetrathiafulvalene Ligands on the Electrical Conductivity of 3D Metal–Organic Frameworks. *Chem. Sci.* **2021**, *12*, 13379–13391.

(92) Wang, T.; Vermeulen, N.; Kim, I. *S.*; Martinson, A. B. F.; Stoddart, J. F.; Hupp, J. T.; Farha, O. K. Scalable synthesis and post-modification of a mesoporous metal-organic framework called NU-1000. *Nat. Protoc*. **2016**, *11,* 149–162.

(93) Peng, L.; Yang, S.; Sun, D. T.; Asgari, M.; Queen, W. L. MOF/polymer composite synthesized using a double solvent method offers enhanced water and CO_2 adsorption properties. *Chem. Commun.* **2018**, *54*, 10602–10605.

Table of Contents